AMERICAN SOCIETY FOR MICROBIOLOGY | Molecular and Cellular Biology®

RESEARCH ARTICLE

Active Replication Checkpoint Drives Genome Instability in Fission Yeast *mcm4* Mutant

Seong Min Kim,[a] Susan L. Forsburg[a]

[a]Molecular and Computational Biology, University of Southern California, Los Angeles, California, USA

ABSTRACT Upon replication fork arrest, the replication checkpoint kinase Cds1 is stimulated to preserve genome integrity. Robust activation of Cds1 in response to hydroxyurea prevents the endonuclease Mus81 from cleaving the stalled replication fork inappropriately. However, we find that the response is different in temperature-sensitive *mcm4* mutants, affecting a subunit of the MCM replicative helicase. We show that Cds1 inhibition of Mus81 promotes genomic instability and allows *mcm4-dg* cells to evade cell cycle arrest. Cds1 regulation of Mus81 activity also contributes to the formation of the replication stress-induced DNA damage markers replication protein A (RPA) and Ku. These results identify a surprising role for Cds1 in driving DNA damage and disrupted chromosomal segregation under certain conditions of replication stress.

KEYWORDS Cds1, Chk1, Mus81, checkpoint kinase, fission yeast, genome stability, mcm4, replication stress

Replication stress increases the likelihood of gross chromosome rearrangements, micronucleus formation, and chromothripsis observed in various cancers (reviewed in references 1 to 3). During replication, the conserved MCM helicase, comprising six subunits, unwinds the DNA duplex and promotes replication initiation and progression (4). Mutations in Mcm4, one of the subunits of the MCM helicase, have been implicated in various cancers, including breast cancer and leukemia (5–10).

In fission yeast, temperature-sensitive alleles of the *mcm4* gene have been useful in modeling replication dynamics and replication stress (11–14). The originally isolated *mcm4-M68* (*mcm4-ts*) mutant (15) is a temperature-sensitive mutant that undergoes substantial DNA synthesis, accompanied by the accumulation of double-strand breaks (DSBs) that activate the damage checkpoint kinase Chk1 at restrictive temperature (36°C) (12, 16, 17). In contrast, the *mcm4-ts-dg* (*mcm4-dg*) mutant has a degron cassette added to the original temperature-sensitive allele that causes rapid protein turnover at 36°C (18). Unlike the *mcm4-ts* mutant, *mcm4-dg* cells evade Chk1 activation and continue to divide despite having drastically underreplicated DNA content at 36°C (12). This results in uneven DNA segregation that generates ultrafine anaphase bridges, lagging chromosomes, and micronuclei (12).

Upon replication stress, single-stranded DNA (ssDNA) is generated from the uncoupling of the helicase from the replisome and subsequent resection (19–22). The ssDNA-binding protein replication protein A (RPA) is then recruited to initiate the recruitment of damage response proteins and activate the appropriate response (23). The slowing or stalling of replication fork progression, for example, by treatment with hydroxyurea (HU), which depletes deoxynucleoside triphosphate (dNTP) pools, activates the replication checkpoint kinase Cds1, which has multiple substrates to restrain cell cycle progression and promote fork repair and restart (24–26; reviewed in reference 27).

Fission yeast Cds1 is recruited to stalled replication forks and phosphorylated by

Citation Kim SM, Forsburg SL. 2020. Active replication checkpoint drives genome instability in fission yeast *mcm4* mutant. Mol Cell Biol 40:e00033-20. https://doi.org/10.1128/MCB.00033-20.

Address correspondence to Susan L. Forsburg, forsburg@usc.edu.

Received 24 January 2020
Returned for modification 24 March 2020
Accepted 17 April 2020
Accepted manuscript posted online 27 April 2020
Published 29 June 2020

DNA-dependent protein kinase-like family Rad3, which promotes dimerization and further activation by autophosphorylation (28, 29). Cds1 interacts with and regulates the Mus81-Eme1 structure-specific endonuclease complex that cleaves a variety of DNA structures, including stalled replication forks (27, 30–33; reviewed in reference 34). Cds1 activation releases Mus81 from the chromatin and thus prevents the inappropriate cleavage of the stalled replication fork (33). This helps limit Mus81 activity in S phase. Rather, Mus81 appears particularly important for the resolution of entanglements entering mitosis (reviewed in reference 35).

In this study, we show that Cds1 kinase and its regulation of Mus81 contribute to the evasion of the DNA damage checkpoint and allow uneven nuclear division in *mcm4-dg* cells. We demonstrate that Mus81 influences the formation of cytological markers of replication stress, including enlarged single RPA puncta (megafoci) observed in *mcm4-dg* cells. These RPA megafoci in *mcm4-dg* cells form at the nuclear periphery from the coalescence of smaller, multicluster RPA, dependent on the DNA-end-binding heterodimer protein Ku. Our findings thus suggest that under some conditions of replication stress, an active replication checkpoint contributes to genome instability, generating novel structures inside the nucleus.

RESULTS

Cds1 regulation of Mus81 promotes genomic instability in early replication failure. The *mcm4-M68-ts* (*mcm4-ts*) mutant allele of the MCM helicase undergoes robust cell cycle arrest at the restrictive temperature, with the presence of DNA double-strand breaks (DSBs) and activation of the damage checkpoint kinase Chk1 (12, 17, 36). Previously, we showed that *mus81*Δ bypasses mitotic arrest and increases uneven nuclear divisions in temperature-sensitive *mcm4-ts* cells (12). We proposed that the DNA breaks induced by Mus81 in *mcm4-ts* cells are sufficient to activate the Chk1 damage checkpoint, leading to cell cycle arrest (12).

The replication checkpoint kinase Cds1 downregulates Mus81 activity by promoting its dissociation from chromatin upon hydroxyurea (HU) treatment (33). Thus, the activation of Cds1 by prior treatment with HU should have an effect similar to that of *mus81* deletion in *mcm4-ts* cells. We confirmed our previous observation (17) that pretreatment of *mcm4-ts* cells with HU increases uneven DNA segregation, generating cut (unreplicated DNA cleaved by the septum) or aneuploid phenotypes (Fig. 1A).

This increase in nuclear division in *mus81*Δ *mcm4-ts* or HU-treated *mcm4-ts* cells resembles the phenotype of the temperature-sensitive degron allele *mcm4-ts-dg* (*mcm4-dg*) that we showed previously is able to evade the Chk1 damage checkpoint (12) (Fig. 1A). Importantly, pretreatment with HU does not increase abnormal division in *mcm4-dg* cells (Fig. 1A). From these data, we infer that the *mcm4-dg* mutant already induces sufficient Cds1 activity at the restrictive temperature that is sufficient to downregulate Mus81, allowing it to prevent the damage that induces the Chk1 checkpoint.

Consistent with this model, we find that *cds1*Δ *mcm4-dg* cells have a reduced frequency of abnormal nuclear division at 36°C. Significantly, this reduction depends upon Mus81 (Fig. 1B), suggesting that Cds1-dependent downregulation of Mus81 allows *mcm4-dg* cells to proceed into mitosis. We tested this using separation-of-function mutations in Cds1 and Mus81. Mutations in the forkhead-associated (FHA) domain of Cds1 (*cds1-FHA**) or the FHA-binding site on Mus81 (*mus81-T239A*) prevent the interaction between Cds1 and Mus81 (33, 37). We predicted that these mutations should phenocopy *cds1*Δ by blocking the Cds1 interaction with and inhibition of Mus81, and indeed, this is the case. Both the *cds1-FHA* mcm4-dg* and *mus81-T239A mcm4-dg* double mutants decreased the frequency of abnormal division in the *mcm4-dg* background, measured by cut and aneuploid cells (Fig. 1C).

We next predicted that increasing Cds1 activity in *mcm4-ts* cells should phenocopy the abnormal divisions of the *mus81*Δ *mcm4-ts* strain by repressing Mus81. Indeed, we find that the overexpression of Cds1 in *mcm4-ts* cells increases uneven nuclear division, and this requires an intact kinase domain (Fig. 1D). These findings indicate that under

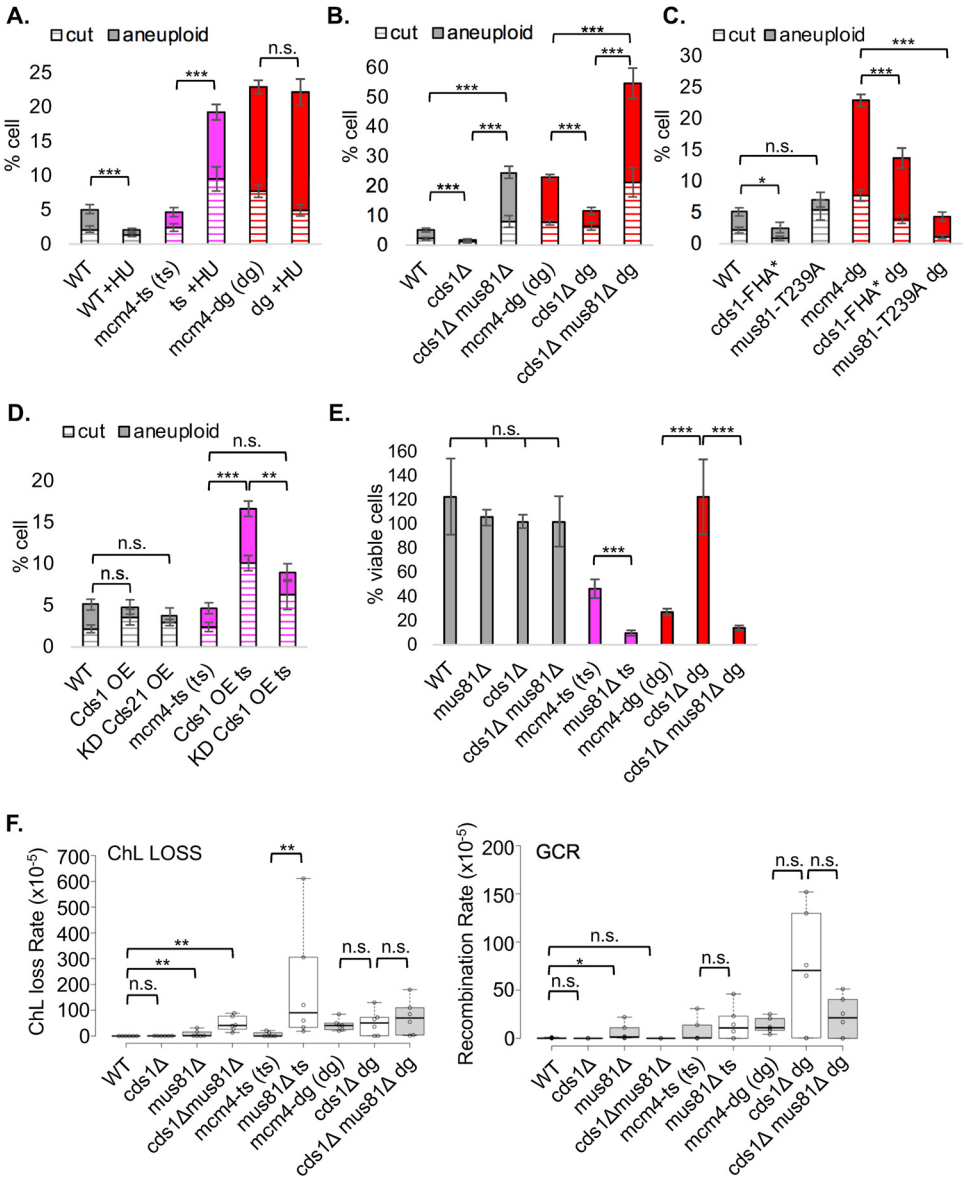

FIG 1 Cds1 regulation of Mus81 contributes to uneven chromosomal segregation in *mcm4* mutants. (A) Asynchronous cultures of WT, *mcm4-ts*, and *mcm4-dg* cells were placed at 36°C for 4 h, or pretreated with 12 mM HU for 2 h and then placed at 36°C for 4 h, and fixed for DAPI staining. Cells with cut or aneuploid nuclei were quantified. (B and C) The indicated cells were placed at 36°C for 4 h and fixed for DAPI staining. (D) WT Cds1 or kinase-dead (KD) Cds1 was overexpressed (OE) in the indicated cells, placed at 36°C for 4 h, and fixed for DAPI staining. Shown are averages from at least 3 replicates, with >50 cells counted per replicate. (E) The indicated cells were placed at 36°C for 4 h, plated on a YES plate, and grown at 25°C. Shown are averages from 6 replicates. (F) Rates of minichromosome (ChL) loss or gross chromosomal rearrangement (GCR) in the indicated cells after 4 h at 36°C. *, $P < 0.05$; **, $P < 0.01$; ***, $P < 0.001$; n.s., not significant. Error bars represent SE.

some forms of replication stress, an active replication checkpoint kinase, Cds1, drives catastrophic mitosis and chromosome instability.

The frequency of abnormal chromosome segregation correlates with reduced viability in *mcm4-dg* compared to *mcm4-ts* cells (12). We find that viability likewise correlates with Cds1 regulation of Mus1 activity. The loss of viability in the *mus81Δ mcm4-ts* mutant correlates with increased divisions, and the increased viability in the *cds1Δ mcm4-dg* mutant that requires Mus81 correlates with reduced divisions (Fig. 1E).

We assessed the contributions of Mus81 to chromosome loss and rearrangement using strains that contain a nonessential minichromosome (ChL) (12, 38). ChL carries multiple genetic markers that are used to distinguish chromosome loss from structural

rearrangement. Briefly, ChL loss results in the loss of all genetic markers, leading to multiple auxotrophies and hygromycin sensitivity, while gross chromosomal rearrangement (GCR) results in the loss of some but not all markers (see Materials and Methods). As we showed previously, there are increased rates of both chromosome loss and GCR in the *mcm4-dg* strain compared to the *mcm4-ts* strain after a 4-h pulse at 36°C (Fig. 1F) (12). However, while *mus81*Δ dramatically increased the rate of ChL loss in the *mcm4-ts* strain, it only mildly increased the rate of GCR. Conversely, Cds1 deletion in the *mcm4-dg* strain did not have a significant effect on the ChL loss rate but increased the GCR rate in a Mus81-dependent manner. Thus, the consequence of Mus81 activation in late-S-phase arrest (*mcm4-ts*) compared to early replication failure (*cds1*Δ *mcm4-dg*) has different genetic outcomes.

Cds1 in the *mcm4-dg* strain inhibits Mus81 contribution to Chk1 activation. Compared to *mcm4-ts* cells, *mcm4-dg* cells have reduced Chk1 activation and evade Chk1-dependent cell cycle arrest (12). We posited that Mus81-generated DSBs are responsible for Chk1 activation in the *mcm4-ts* mutant. Consistent with this, we observed more chromatin-bound Mus81 in the *mcm4-ts* mutant than in the *mcm4-dg* mutant (Fig. 2A) and a reduction of Chk1 phosphorylation in the *mus81*Δ *mcm4-ts* mutant but an increase in the *cds1*Δ *mcm4-dg* mutant compared to the single mutants (Fig. 2B). DNA damage induces the phosphorylation of the histone variant H2A, which recruits the DNA repair protein Crb2 and facilitates Chk1 activation (39). Again, consistent with Chk1 activation, we found that the *mcm4-ts* mutant has more phosphorylated H2A (pH2A) than the *mcm4-dg* mutant at the restrictive temperature (Fig. 2C). The loss of Mus81 decreased pH2A in the *mcm4-ts* mutant, and the loss of Cds1 regulation of Mus81 increased pH2A in the *mcm4-dg* mutant. Thus, Mus81 activity correlates with Chk1 activation.

Cds1 regulation of Mus81 contributes to the distinct formation of aberrant DNA damage markers. Our data thus far indicate different outcomes if Mus81 is activated in cells with early replication defects compared to late-S-phase/G_2 arrest. Mus81 processes replication-associated DNA structures for repair and fork progression (40–43), and intermediates formed during this process may generate Chk1-activating DNA structures. As previously shown, the *mcm4-ts* and *mcm4-dg* mutants have distinctive RPA cytological phenotypes (12). *mcm4-ts* cells after 4 h at 36°C contain small and multicluster RPA puncta, while *mcm4-dg* cells have single RPA foci that are large and more intense, which we refer to as "megafoci" (12) (Fig. 3B). We reasoned that these cytological markers may give us insights into the structures recognized or created by Mus81 and the response that they trigger.

First, we investigated the recruitment of another marker. DNA ends are recognized by the Ku heterodimer proteins that promote nonhomologous end joining (NHEJ) (44–46). Ku also recognizes "one-sided" double-strand breaks and ends associated with regressed replication forks (47, 48). Ku binding of DNA ends inhibits resection and the accumulation of single-stranded DNA (ssDNA) that otherwise drives homologous recombination (HR) (44). Ku proteins also play important roles in replication fork reversal and restart by regulating fork resection and facilitating RPA loading (49). Recently, we identified a distinct pattern of Ku focus formation in response to genotoxic stress (C. Jones, personal communication). We observe that at the restrictive temperature, *mcm4-dg*, but not *mcm4-ts*, cells have visible Ku foci (Fig. 3A). We reasoned that Ku is not efficiently removed from DNA ends in *mcm4-dg* cells, which could inhibit HR-mediated attempts at fork restart.

Next, we investigated the contribution of Mus81 to these phenotypes. We observed that the loss of Mus81 in the *mcm4-ts* mutant phenocopies the cytological markers of the *mcm4-dg* mutant, with an increased Ku signal and megafocus RPA (Fig. 3C and D), and this correlates with the increase in abnormal divisions (Fig. 1) (12). Conversely, the *cds1*Δ *mcm4-dg* mutant shows less intense, multicluster RPA foci similar to those seen in the *mcm4-ts* mutant. Finally, *cds1*Δ *mus81*Δ *mcm4-dg* triple mutants have single but small RPA foci. We found that *cds1*Δ also decreases Ku focus size in *mcm4-dg* cells in a Mus81-dependent manner (Fig. 3E). Thus, a distinct fingerprint of cytological markers

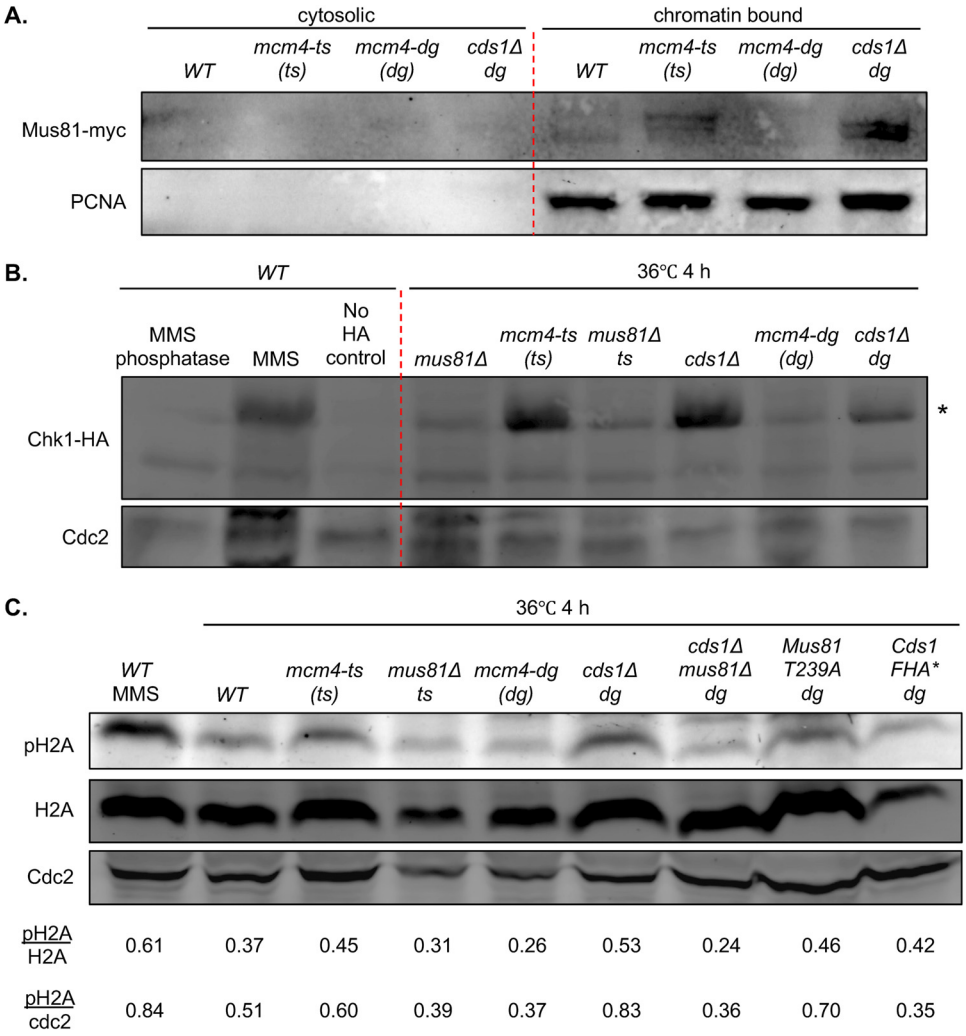

FIG 2 Cds1 regulation of Mus81 inhibits Chk1 activation in *mcm4-dg* cells. (A) Western blot showing chromatin-bound Mus81 in *mcm4* mutants. Chromatin fractionation prepared from cells placed at 36°C for 4 h is shown. PCNA is shown for the nuclear fraction. (B) Western blot showing the HA-tagged Chk1 phosphorylation shift. The third lane is the control lysate that contains no Chk1-HA. The second lane is the lysate from Chk1-HA-containing WT cells treated with 0.007% methyl methanesulfonate (MMS). The first lane is the phosphatase-treated lysate from Chk1-HA-containing WT cells treated with MMS. The remaining lanes are lysates from the indicated cells placed at 36°C for 4 h. * indicates phospho shifted Chk1. Cdc2 is the loading control. (C) Western blot showing phospho-H2A and H2A. Cdc2 is the loading control. The first lane is the lysate from WT cells treated with 0.007% MMS. The remaining lanes are lysates from the indicated cells placed at 36°C for 4 h. Quantification of band intensities was performed using ImageJ, and the ratios of phospho-H2A over H2A or Cdc2 are shown.

accompanies the different phenotypes, and this correlates with Mus81 and Cds1 activity. This may represent different forms of DNA damage processing in the different mutant backgrounds.

Ku contributes to the relocation of DNA lesions to the nuclear periphery and megafocus RPA formation. We next examined the dynamics of focus and megafocus formation using time-lapse imaging of RPA and Ku in *mcm4-dg* cells. We shifted asynchronous cultures to the restrictive temperature and monitored multiple markers. We normalized the data to the time at which the first septation occurs. The majority of cycling cells (at 25°C) are in G_2, and septation typically correlates with S phase (50); thus, in a temperature shift experiment, we expect that the inactivation of the essential S-phase protein Mcm4 will have an effect as cells enter S phase. Consistent with this, we observed that RPA appears near the time of septation in dispersed small clusters. Intriguingly, these clusters merge to form megafocus RPA (Fig. 4A and B; see also Movie

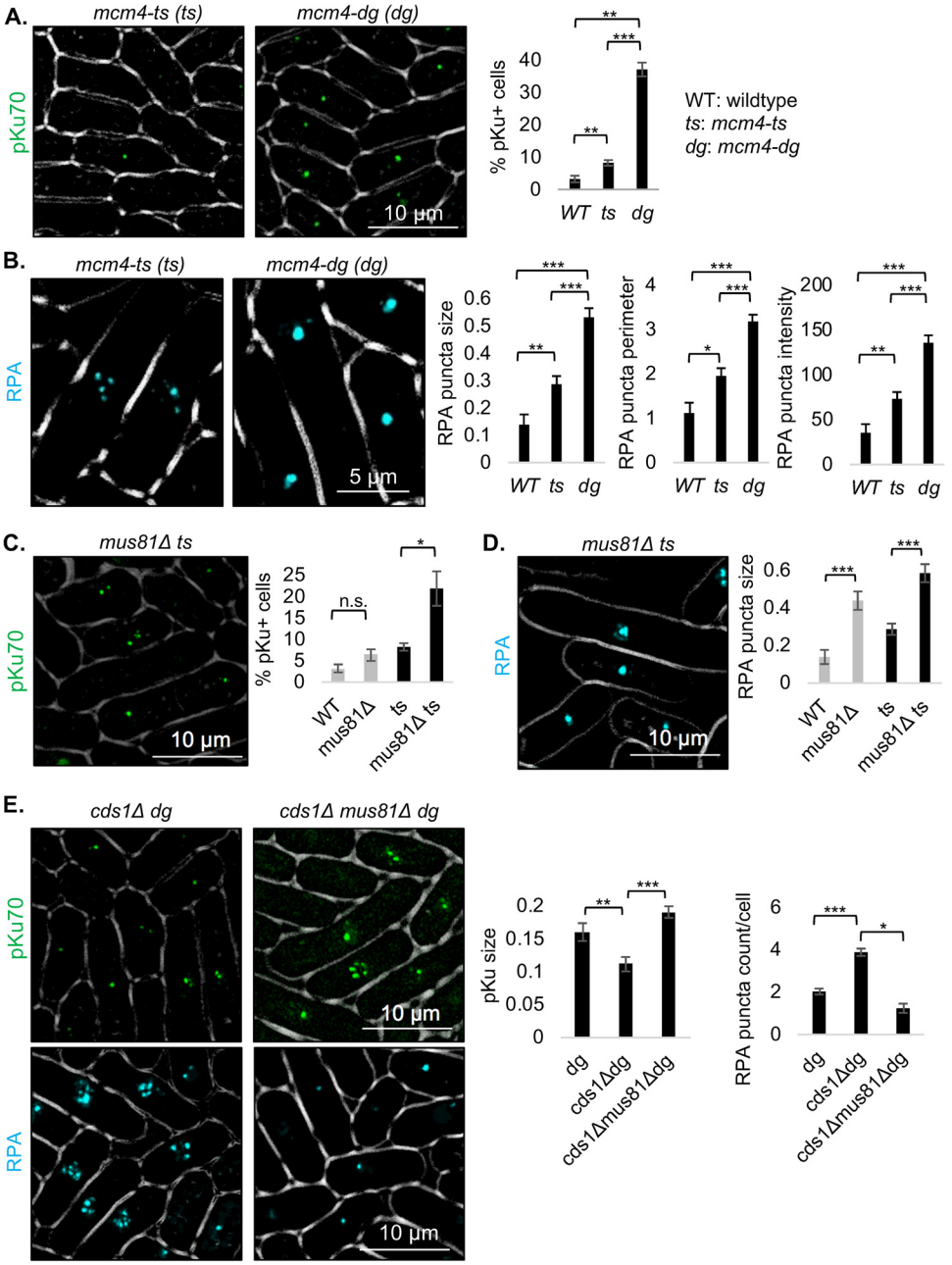

FIG 3 Cds1 regulation of Mus81 contributes to DNA damage marker focus formation in *mcm4* mutants. (A and C) Cells were imaged for pKu70-citrine after 4 h at 36°C. Percentages of T cells with pKu70 foci are quantified on the right. (B and D) Cells were imaged for RPA-cyan fluorescent protein (CFP) after 4 h at 36°C. Quantifications of RPA focus size (square micrometers), perimeter (micrometers), and intensity (area times the mean gray value) are on the right. (E) Cells were imaged for pKu70-citrine or RPA-CFP after 4 h at 36°C. Quantifications of pKu70 focus size (square micrometers) and the number of RPA foci per cell are on the right ($n > 200$ cells). *, $P < 0.05$; **, $P < 0.01$; ***, $P < 0.001$; n.s., not significant. Error bars represent SE.

S1 in the supplemental material). Ku also appears around the time of RPA multifoci in one or two foci, which persist into the RPA megafoci.

The deletion of either *cds1* alone or both *cds1* and *mus81* only slightly altered the timing of the appearance of multifocus RPA or Ku (Fig. 4C), but these strains do not form megafoci (e.g., see Fig. 3E). Changes in uneven nuclear division, viability, gross chromosomal rearrangement, RPA focus size (Fig. 1 and Fig. 3E), and the timing of RPA multifoci in Cds1-deleted *mcm4-dg* cells are reversed by *mus81* deletion (Fig. 4C), indicating a crucial role for this endonuclease in creating these structures. Interestingly,

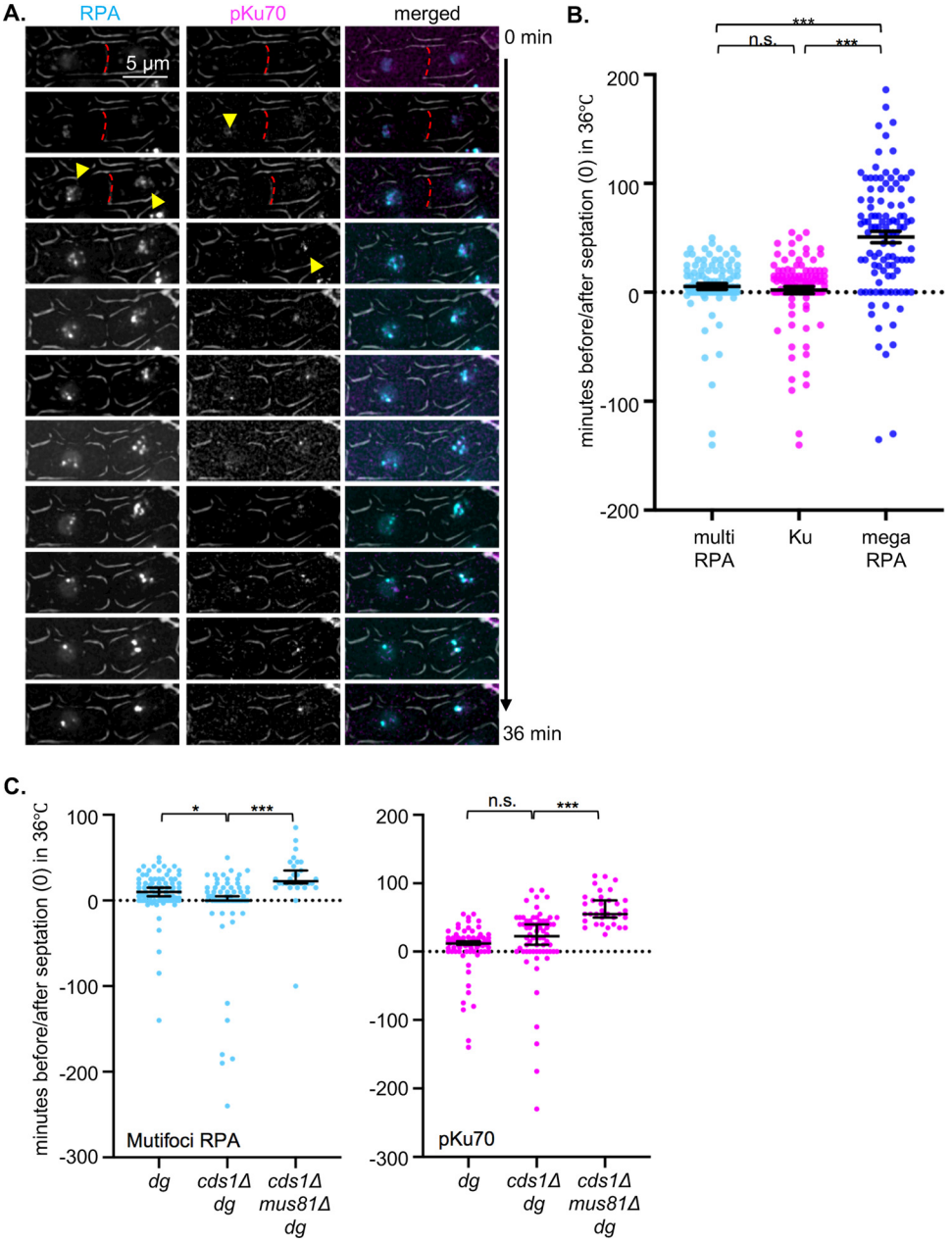

FIG 4 Multicluster RPA and Ku come together to form RPA megafoci. (A) *mcm4-dg* cells were imaged over time at 36°C for RPA-CFP and pKu-citrine. The dashed lines indicate septation. The arrowheads indicate the initial appearance of foci. (B) Timing of the appearance of foci relative to septation (dotted line) from cells imaged as described above for panel A. (C) Timing of the appearance of multifocus RPA and Ku in the indicated strains placed at 36°C relative to septation. *, $P < 0.05$; ***, $P < 0.001$; n.s., not significant. Error bars represent SE.

although the decrease in Ku focus size in *cds1*Δ *mcm4-dg* cells is reversed in *cds1*Δ *mus81*Δ *mcm4-dg* cells, the timing of the Ku appearance was slightly delayed in *cds1*Δ *mcm4-dg* cells and further delayed in *cds1*Δ *mus81*Δ *mcm4-dg* cells (Fig. 4C). Thus, there may be an effect of Mus81 on timing independent of Cds1.

Several types of DNA lesions, including DSBs and collapsing forks, relocate to the nuclear periphery for repair (reviewed in references 51 and 52). We observed that RPA multifoci in *mcm4-dg* cells are found at the center of the nucleus, while megafocus RPA is generally located near the periphery, colocalizing with or in close proximity to the nuclear membrane-associated proteins Ccr1N, Nup107, and Ish1 (Fig. 5A to C). Similarly, we find that RPA multifoci in *mcm4-ts* cells are located mostly near the center of the

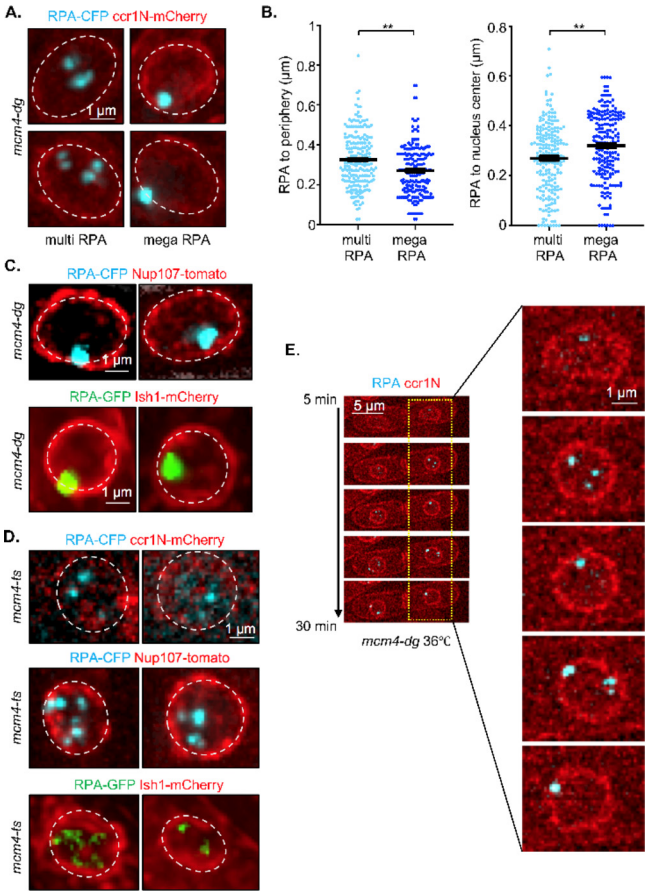

FIG 5 Multicluster RPA moves to the nuclear periphery to form megafoci. (A) *mcm4-dg* cells were imaged for RPA-CFP and ccr1N-mCherry after 4 h at 36°C. The dotted lines outline the nucleus. (B) Quantification of the distance between the center of each RPA focus and the nearest ccr1N or nucleus center from the images in panel A. (C) *mcm4-dg* cells were imaged for RPA-CFP and Nup107-tomato or for RPA-green fluorescent protein (GFP) and Ish1-mCherry after 4 h at 36°C. (D) *mcm4-ts* cells were imaged for the indicated fluorophores after 4 h at 36°C. (E) *mcm4-dg* cells were imaged for RPA-CFP and ccr1N-mCherry over time at 36°C. **, $P < 0.01$. Error bars represent SE.

nucleus (Fig. 5D). Time-lapse imaging showed that RPA multifoci form near the center of the nucleus and relocate to the nuclear periphery as they coalesce to form megafocus RPA (Fig. 5E and Movie S2).

We next examined whether Ku influences the relocalization of the RPA puncta into the peripheral megafocus. Neither *pku70*Δ nor wild-type (WT) cells accumulate any RPA foci at the restrictive temperature. *pku70*Δ *mcm4-dg* cells show an increase in RPA multifoci (Fig. 6A). These RPA multifoci in *pku70*Δ *mcm4-dg* cells do not relocate to the nuclear periphery and do not coalesce into megafoci (Fig. 6B and C). They appear similar to RPA multifoci in *mcm4-ts* cells (Fig. 6D). These data indicate that Ku contributes to megafocus RPA formation and relocalization.

We assessed the contribution to these phenotypes of other nucleases and helicases that contribute to DNA damage and its resolution (Table 1). We observed that deletion of the long-range exonuclease gene *exo1* in the *mcm4-dg* mutant does not rescue uneven chromosomal segregation, although it increases multifocus RPA and decreases Ku localization (Fig. 7). Overall, a decrease in Ku foci in the *mcm4-dg* background correlates with an increase in multifocus RPA (Table 1).

DISCUSSION

In this report, we describe the mechanistic basis for different cell cycle phenotypes associated with two temperature-sensitive alleles of the MCM helicase in *Schizosaccha-*

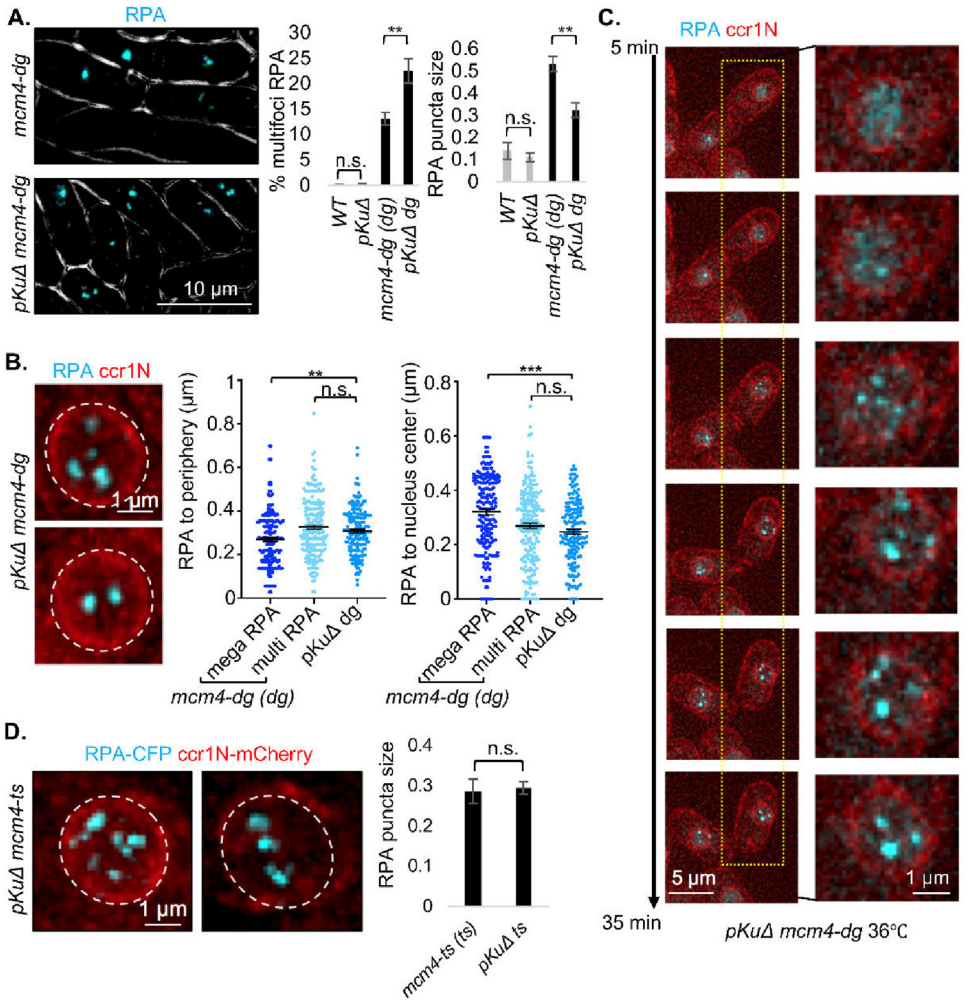

FIG 6 Ku promotes relocation of multicluster RPA to the nuclear periphery to form megafoci. (A, left) *mcm4-dg* and pKu70-deficient *mcm4-dg* cells were imaged for RPA-CFP. (Right) Percentages of cells with RPA multifoci out of the RPA-containing population and quantification of RPA focus sizes (square micrometers) ($n > 200$). (B, left) pKu70-deficient *mcm4-dg* cells were imaged for RPA-CFP and ccr1N-mCherry after 4 h at 36°C. Dashed lines outline the nucleus. (Right) Quantification of the distance between the center of each RPA focus and the nearest ccr1N or nucleus center. (C) pKu70-deficient *mcm4-dg* cells were imaged over time at 36°C for RPA-CFP and ccr1N-mCherry. (D, left) pKu70-deficient *mcm4-ts* cells were imaged for RPA-CFP and ccr1N-mCherry after 4 h at 36°C. (Right) Average RPA punctum sizes (square micrometers) ($n > 200$). **, $P < 0.01$; ***, $P < 0.001$; n.s., not significant. Error bars represent SE.

romyces pombe: *mcm4-ts*, which arrests the cell cycle with 2C DNA content, and *mcm4-dg*, which fails to arrest the cell cycle despite the absence of substantial DNA synthesis (12). We showed previously that *mcm4-ts* cells evade cell cycle arrest if the structure-specific endonuclease Mus81 is deleted (12). Here, we identified a key role for the Cds1 replication checkpoint kinase that represses Mus81 (33, 37). Our data suggest that the DSBs that occur in *mcm4-ts* cells reflect a lack of Cds1 activation, which allows Mus81 cleavage of the DNA that is sufficient to activate the Chk1 damage checkpoint and causes cell cycle arrest (Fig. 8).

Our model further suggests that Mus81 is not active in *mcm4*-dg cells, because they do not activate a DSB response and do not arrest the cell cycle (12, 17). We find that the inactivation of Mus81 is Cds1 dependent. In contrast, separation-of-function mutations in *cds1* or *mus81* that prevent their protein interaction with each other result in cell cycle arrest in *mcm4-dg* cells. These observations suggest that the Cds1 replication checkpoint kinase is activated in *mcm4-dg* cells sufficiently to inhibit Mus81 and prevent the formation of DSBs. This in turn evades the activation of Chk1, allowing cells

TABLE 1 Percentages of pKu70 focus-containing cells and RPA focus sizes[a] in *mcm4-dg* cells with deletions of various proteins involved in replication stress and DNA repair

Allele[b]	Protein function[c]	Change in % pKu focus-positive cells[d]	Change in RPA focus size
crb2Δ	DNA repair protein	Decrease	Decrease in size with increased multifoci
ctp1Δ	Endonuclease	Decrease	Decrease in size with increased multifoci
dna2-ts	Endonuclease-helicase	Increase	Decrease in size with increased multifoci
exo1Δ	Exonuclease	Decrease	No change in size with increased multifoci
kpa1Δ	DNA repair polymerase	No change	No change
mre11Δ	Nuclease in HR	Decrease	Decrease in size
pKu70Δ	DNA binding in DNA repair	Not applicable	Decrease in size with increased multifoci
rad16Δ	DNA repair endonuclease	Decrease	No change
rad2Δ	FEN-1 endonuclease	Slight decrease	No change
rad8Δ	Ubiquitin ligase/DNA helicase	Decrease	Decrease in size with increased multifoci
rif1Δ	Telomere length regulator	No change	Decrease in size with increased multifoci
slx4Δ	Structure-specific endonuclease	Decrease	No change
swi10Δ	DNA repair endonuclease	Slight decrease	Slight decrease

[a]For RPA size in *mcm4-dg* cells, "multifoci" indicates an increase in the overall percentage of multifocus RPA-containing cells.
[b]Alleles in boldface type are ones that show a trend in which a decrease in pKu foci is correlated with a decrease in RPA megafoci (increase in RPA multifoci) in *mcm4-dg* cells.
[c]Protein function from pombase.org (86).
[d]Slight decrease indicates a decrease within a 10 to 20% difference. Differences of >20% are indicated as an increase or decrease.

to proceed into mitotic division in the absence of replication, with disastrous consequences. Thus, paradoxically, the activation of the replication checkpoint in the *mcm4-dg* mutant causes, rather than prevents, genome instability.

However, we do not observe an obvious phosphorylation mobility shift of Cds1 in the *mcm4-dg* mutant (12), which would typically be observed if the replication checkpoint is activated by treatment with hydroxyurea that results in cell cycle arrest (e.g., see references 24 and 26). This suggests that the level of Cds1 activation sufficient to inhibit Mus81 in the *mcm4-dg* mutant (Fig. 2) does not require substantial phosphorylation. There is additional evidence that suggests that Cds1 is not activated to its full level under these conditions. In HU, Cds1 kinase upregulates the G_1/S-phase master transcription factor MBF (MluI-binding factor transcriptional complex) (53–56) and the MBF target protein Tos4 (54, 57). We showed recently that Cds1 activity in the*mcm4-dg* cells does not induce Tos4 accumulation (58). These data suggest that a partial activation of Cds1 is occurring in *mcm4-dg* cells.

We cannot rule out the possibility that the cell cycle stage contributes to the different Mus81-associated phenotypes observed in *mcm4* mutants. The robust regulation of Mus81 by Cds1 in *mcm4-dg* but not in *mcm4-ts* cells could reflect an early-S-phase failure in the degron compared to a late-S-phase or even G_2 defect in *mcm4-ts* cells (see discussion in reference 56). However, we consider this unlikely, because the *mus81Δ mcm4-ts* mutant, which completes substantial DNA synthesis, resembles the *mcm4-dg* mutant in divisions and cytological phenotypes, despite the difference in DNA content.

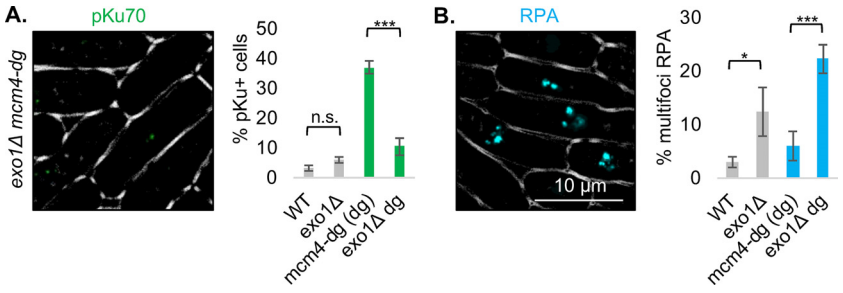

FIG 7 Exo1 deletion effect in *mcm4-dg* cells. Cells were imaged for pKu70-yellow fluorescent protein (YFP) (A) and RPA-CFP (B) after 4 h at 36°C. On the right of the images are quantifications of the percentages of Ku focus-containing cells or of the percentages of multifocus RPA-containing cells out of the RPA-containing population ($n > 200$). *, $P < 0.05$; ***, $P < 0.001$; n.s., not significant. Error bars represent SE.

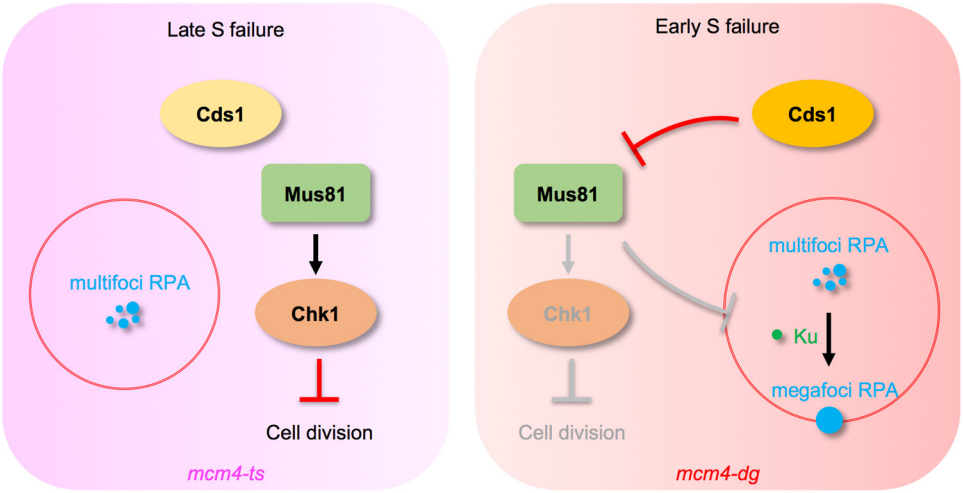

FIG 8 Model figure illustrating the contribution of Cds1 regulation of Mus81 to Chk1 activation and RPA focus formation in *mcm4* mutants. *mcm4-ts* cells that have late replication failure do not have robust Cds1 activation, and therefore, Mus81 remains active. RPA multifoci appear near the center of the nucleus, while Ku is likely processed and does not accumulate in a Mus81-dependent manner. Active Mus81 also contributes to Chk1-dependent cell cycle arrest. *mcm4-dg* cells that have early replication failure have Cds1 activation and subsequent downregulation of Mus81. RPA multifoci appear early near the center of the nucleus along with Ku and relocate to the nuclear periphery to form RPA megafoci. The lack of Mus81 activation of Chk1 allows evasion of cell cycle arrest, resulting in chaotic chromosomal segregation.

Our observations are also consistent with previous reports that Cds1-dependent Mus81 regulation may be differentially activated depending on the type or extent of replication stress, with HU-induced stress being the most pronounced (33, 59, 60). In a DNA polymerase alpha mutant at the semipermissive temperature, Cds1 is sufficiently active to inhibit Mus81 (33, 59, 61). Mus81 activity in *cds1*Δ *pol1* cells causes breaks that generate genome rearrangement. Intriguingly, the *mus81-T239A* point mutant that is independent of Cds1 does not cause breaks in HU (59), in contrast to what is seen in the *mcm4-dg* or *pol1* background (Fig. 1) (33, 59). Thus, the activation of the checkpoint by HU (nucleotide starvation) does not phenocopy stresses caused by replisome defects.

This difference in HU treatment versus replisome defects is consistent with our observations in the *mcm4* mutants. While *mus81*Δ dramatically increases the rate of ChL loss in *mcm4-ts* cells, it only mildly increases the rate of GCR. This is consistent with a known requirement for Mus81 to segregate entangled chromosomes in mitosis (reviewed in reference 35): the *mcm4-ts* mutant has a largely replicated genome, so a failure to disentangle sister chromatids may generate a chromosome loss phenotype. Conversely, Cds1 deletion in the *mcm4-dg* mutant did not have a significant effect on the ChL loss rate but increased the GCR rate in a Mus81-dependent manner. The *mcm4-dg* mutant has a largely unreplicated genome; thus, unscheduled Mus81 cleavage drives rearrangement rather than segregation errors. These results suggest that Mus81 inhibits chromosome loss in late replication failure, whereas Mus81 promotes gross chromosomal rearrangement in early replication failure.

Does this implicate Cds1 in normal S-phase progression? Cds1-deficient cells accumulate DNA damage foci even without HU treatment (62) and also show altered replication dynamics (63). These data suggest that Cds1 has a role in maintaining genome stability even in an unperturbed S phase, perhaps by ensuring that Mus81 is not activated during normal DNA replication. This agrees with the data suggesting that Mus81 activity is most prominent during mitosis to resolve entanglements and promotes mitotic DNA synthesis (reviewed in references 34 and 64). Boddy et al. (37) reported that the *mus81*Δ mutant has a checkpoint-dependent cell cycle delay, and Kai et al. (33) showed that the *mus81*Δ mutant has an increased mutation rate, particularly rearrangement between short repeats, in unperturbed cells. These observations are

consistent with Mus81's normal mitotic function and error-prone recombination becoming active in its absence. We propose that the *mcm4-dg* phenotype reflects this maintenance level of Cds1 activity, which is not enough to induce Tos4 expression or prevent cell cycle progression but is sufficient to inhibit Mus81. In contrast, the failure of Cds1 to downregulate Mus81 in *mcm4-ts* cells indicates that these cells with mostly 2C DNA content may be arrested not at S phase but at G_2 phase, which will also explain their lack of Tos4 accumulation (58).

In addition to the dynamics of Cds1 and Mus81, we identified a unique visual fingerprint of *mcm4-dg* genome stress using fluorescently tagged repair proteins. RPA-coated ssDNA recruits Rad3 and initiates checkpoint activation (65, 66). Additionally, 5′ single-stranded/double-stranded DNA junctions and primer-template junctions are required for strong Chk1 activation (2, 22, 67–69). *mcm4-dg* cells have large RPA megafoci but do not activate Chk1 (12), suggesting that other Chk1-activating DNA structures beyond ssDNA are missing. Mus81 processes replication-associated DNA structures for repair and fork progression (40–43), and intermediates formed during this process may generate Chk1-activating DNA structures, so this is consistent with the absence of Mus81 cleavage in *mcm4-dg* cells. The lack of Mus81 activity in *mcm4-dg* cells likely results in accumulation of unresolved recombination intermediates such as D-loops or other unusual DNA structures such as hairpins and triplexes as well as subsequent chromosome breaks (70, 71).

So what is the source of the RPA megafoci? In our time course analysis, we see that the *mcm4-dg* mutant initially shows dispersed RPA foci that coalesce into a megafocus adjacent to the nuclear envelope. In *Drosophila melanogaster* cells, the relocalization of heterochromatic DNA damage for homologous recombination (HR) repair requires the recruitment of heterochromatic proteins Smc5/6 and SUMO-E3 ligases (72) and the activation of nuclear actin and myosin (73). Repair foci have also been observed adjacent to the nuclear envelope in *Saccharomyces cerevisiae* (74), and a new study suggests that coalescing Rad52 foci result from the merging of phase-separated droplets in tubulin-dependent migration (75).

Our study suggests a key role for the end-binding heterodimer Ku in megafocus formation and localization. Ku is typically associated with nonhomologous end joining (NHEJ) (44–46), which is cell cycle regulated (76, 77). Recent studies suggest that the Ku heterodimer binds DNA ends associated with collapsed and regressed replication forks (47–49). The release of Ku proteins from the DNA ends by the Mre11-Rad50-Nbs1 (MRN) protein complex is required for ssDNA-binding protein RPA localization and subsequent activation of the Chk1 checkpoint pathway as well as HR (48, 49). Thus, Ku and MRN act as mutual antagonists: Ku inhibits resection driven by MRN, and MRN removes Ku to facilitate homologous recombination over NHEJ (44, 48, 78, 79). However, Ku deletion partially suppresses the defects associated with *mrn*Δ (47), which argues that it is actively repressing HR (possibly through inhibition of Exo1) and not just providing an NHEJ alternate. We show that *mcm4-dg* cells, but not *mcm4-ts* cells, accumulate Ku foci (Fig. 3A), further suggesting that MRN is not activated for further cleavage and implicating Ku in the recognition and repair of the lesions in these cells.

Interestingly, Ku accumulation does not compromise DNA resection at single-ended DNA double-strand breaks (80). A nick near Ku-bound DNA ends also allows Exo1- or Dna2-dependent long-range resection and RPA-dependent unwinding of duplex DNA (81). The DNA processing that occurs in conjunction with persistent Ku may signal cells to attempt DNA repair at the nuclear periphery. This suggests that megafocus RPA formation may correspond to unprocessed Ku. Further study will be necessary to characterize these structures.

This study demonstrates an unexpected role of the replication checkpoint in driving genome instability in early-S-phase failure accompanied by an unusual pattern of damage response markers. This underscores the importance of investigating the role of checkpoint pathways with the whole cellular context in mind, not limited to just exogenous pathways, and suggests that the active checkpoint may be deleterious to cells in replication stress.

TABLE 2 Yeast strains used in this study

Strain	Genotype
FY527	*h⁻ his3-D1 ade6-M216 ura4-D18 leu1-32*
FY784	*h⁺ cdc21-M68 ura4-D18 leu1-32 ade6-M210 can1-1*
FY1501	*h⁺ Δcds1::ura4⁺ ura4-D18 leu1-32 his3-D1 ade6-M210*
FY3936	*h⁻ cdc21-M68-ts-dg::ura4⁺ ura4-D18 leu1-32 ade6-M210 can1-1*
FY4611	*h⁻ chk1HA(ep) ade6-M216 ura4-D18 leu1-32*
FY4743	*h⁻ rad11-Cerulean::hphMX rad22-YFP-natMX leu1-32 ade6-M210 ura4-D18*
FY4749	*h⁺ Δcds1::ura4⁺ rad11-Cerulean::hphMX rad22-YFP-kanMX leu1-32 ura4-D18 ade6-M216*
FY4788	*h⁻ Δmus81::KanMX ura4-D18 ade6-M210 leu1-32 his7-366*
FY4790	*h⁺ Δcds1::ura4⁺ Δmus81::KanMX ura4-D18 ade6-M210 leu1-32*
FY4819	*h⁻ cdc21-M68 Δmus81::KanMX leu1-32 ura4-D18 ade6-M216*
FY4857	*h⁻ cdc21-M68 rad11-Cerulean::hphMX rad22-YFP-natMX leu1-32 ade6-M210 ura4-D18*
FY5188	*h⁺ ade6-Δ ura4-D18 leu1-32 his1-102 ChL[ubcp4::LEU2::chk1 hph::spccB3.18 spcc1322.09::ura4⁺ ade6⁺]*
FY5277	*h⁻ cdc21-M68-ts-dg::ura4⁺ Δcds1::ura4⁺ rad22-YFP-natMX rad11-CFP-hphMX ade6-M216 leu1-32 ura4-D18*
FY5279	*h⁻ cdc21-M68-ts-dg::ura4⁺ rad22-YFP-natMX rad11-CFP-hphMX ade6-M216 leu1-32 ura4-D18*
FY5323	*h⁺ Δcds1::ura4⁺ Δmus81::kanMX rad11-Cerulean::hphMX rad22-YFP-natMX leu1-32 ade6-M210 ura4-D18*
FY5364	*h⁺ Δexo1::ura4⁺ rad22-YFP::natMX6 rad11-CFP::hphMX6 ura4-D18 leu1-32*
FY5428	*h⁻ Δexo1::ura4⁺ ura4-D18 ade6-M210*
FY5516	*h⁻ cdc21-M68-ts-dg::ura4⁺ Δcds1::ura4⁺ leu1-32 ura4-D18*
FY6355	*h⁻ chk1HA(ep) cdc21-M68 ade6-M216 ura4-D18 leu1-32 can1-1*
FY6489	*h⁻ cdc21-M68-ts-dg::ura4⁺ Δexo1::ura4⁺ ura4-D18*
FY6497	*h⁻ cdc21-M68-ts-dg::ura4⁺ chk1HA(ep) ade6-M216 leu1-32 ura4-D18*
FY8478	*h⁺ Δmus81::KanMX Δcds1::ura4⁺ cdc21-M68-ts-dg::ura4⁺ ura4-D18 leu1-32*
FY8488	*h⁺ pKu70-citrinehph his3-D1 ade6-M210 ura4-D18 leu1-32*
FY8515	*h⁻ Δcds1::ura4⁺ cdc21-M68-ts-dg::ura4⁺ chk1HA(ep) ura4-D18 leu1-32 ade6-M216*
FY8519	*h⁻ cds1-FHA*::2HA6His::ura4⁺::leu1⁺ leu1-32 ura4-D18*
FY8520	*h⁺ mus81-T239A::13MYC::kanMX leu1-32 ura4-D18*
FY8554	*h⁻ mus81-T239A::14MYC::kanMX cdc21-M68-ts-dg::ura4⁺ leu1-32 ura4-D18*
FY8563	*h⁺ cds1-FHA*::2HA6His::ura4⁺::leu1⁺ cdc21-M68-ts-dg::ura4⁺ leu1-32 ura4-D18*
FY8580	*h⁺ pKu70-citrinehph cdc21-M68 ura4-D18 leu1-32*
FY8583	*h⁺ pKu70-citrinehph cdc21-M68-ts-dg::ura4⁺ ura4-D18 leu1-32*
FY8586	*h⁺ pKu70-citrinehph cdc21-M68-ts-dg::ura4⁺ Δcds1::ura4⁺ ura4-D18 leu1-32*
FY8616	*h⁻ pKu70-citrinehph cdc21-M68 mus81::kanMX ura4-D18*
FY8712	*h? pku70::kanr cdc21-M68-ts-dg::ura4⁺ rad22-YFP-natMX rad11-CFP-hphMX leu1-32 ura4-D18*
FY8722	*h⁺ Δmus81::KanMX cdc21-M68 chk1HA(ep) ura4-D18 leu1-32*
FY8769	*h⁻ cdc21-M68-ts-dg::ura4⁺ Δexo1::ura4⁺ rad22-YFP::natMX6 rad11-CFP::hphMX6 ura4-D18*
FY8775	*h⁻ Δexo1::ura4⁺ pKu70-citrinehph ura4-D18 ade6-M210*
FY8831	*h⁻ Δexo1::ura4⁺ cdc21-M68-ts-dg::ura4⁺ pKu70-citrinehph ura4-D18*
FY9245	*h⁻ Δcds1::ura4⁺ Δmus81::kanMX cdc21-M68-ts-dg::ura4⁺ rad11-Cerulean::hphMX rad22-YFP-natMX leu1-32 ura4-D18*
FY9248	*h⁻ Δcds1::ura4⁺ Δmus81::kanMX cdc21-M68-ts-dg::ura4⁺ pKu70-citrinehph ura4-D18*
FY9318	*h⁻ Δcds1::ura4⁺ cdc21-M68-ts-dg::ura4⁺ pKu70-citrinehph rad11-CFP-hphMX ura4-D18 leu1-32*
FY9319	*h⁺ Δcds1::ura4⁺ Δmus81::kanMX cdc21-M68(mcm4)-dg::ura4⁺ pKu70-citrinehph rad11-CFP-hphMX ura4-D18*
FY9351	*h⁺ Δmus81::KanMX Δcds1::ura4⁺ cdc21-M68-ts-dg::ura4⁺ chk1HA(ep) ura4-D18 leu1-32 ade6-M216*
FY9405	*h⁺ cdc21-M68-ts-dg::ura4⁺ arg3⁺::ccr1N-mCherry(D817 aa1–275)::his5⁺ pKu70-citrinehph rad11-Cerulean::hphMX ura4-D18*
FY9430	*h⁻ cdc21-M68 ChL[ubcp4::LEU2::chk1 hph::spccB3.18 spcc1322.09::ura4⁺ ade6⁺] ade6-Δ ura4-D18 leu1-32 ade6-M210*
FY9431	*h⁻ cdc21-M68-ts-dg::ura4⁺ ChL[ubcp4::LEU2::chk1 hph::spccB3.18 spcc1322.09::ura4⁺ ade6⁺] ade6-Δ ura4-D18 leu1-32 ade6-M210*
FY9432	*h⁺ cdc21-M68 Δmus81::KanMX ChL[ubcp4::LEU2::chk1 hph::spccB3.18 spcc1322.09::ura4⁺ ade6⁺] ade6-Δ ura4-D18 leu1-32 ade6-M216*
FY9433	*h⁻ cdc21-M68-ts-dg::ura4⁺ Δcds1::ura4⁺ ChL[ubcp4::LEU2::chk1 hph::spccB3.18 spcc1322.09::ura4⁺ ade6⁺] ade6-Δ leu1-32 ura4-D18 ade6-M210*
FY9435	*h⁺ Δmus81::KanMX Δcds1::ura4⁺ cdc21-M68-ts-dg::ura4⁺ ChL[ubcp4::LEU2::chk1 hph::spccB3.18 spcc1322.09::ura4⁺ ade6⁺] ade6-Δ ade6-M216 ura4-D18 leu1-32*
FY9437	*h⁻ Δcds1::ura4⁺ ChL[ubcp4::LEU2::chk1 hph::spccB3.18 spcc1322.09::ura4⁺ ade6⁺] ade6-Δ ura4-D18 leu1-32 ade6-M210*
FY9438	*h⁻ Δmus81::KanMX ChL[ubcp4::LEU2::chk1 hph::spccB3.18 spcc1322.09::ura4⁺ ade6⁺] ade6-Δ ura4-D18 ade6-M210 leu1-32*
FY9439	*h⁻ Δcds1::ura4⁺ Δmus81::KanMX ChL[ubcp4::LEU2::chk1 hph::spccB3.18 spcc1322.09::ura4⁺ ade6⁺] ade6-Δ ura4-D18 ade6-M210 leu1-32*
FY9444	*h⁺ cdc21-M68-ts-dg::ura4⁺ ish1-mCherry-hphMX rad11::rad11-GFP(KanR) ura4-D18*
FY9446	*h⁻ cdc21-M68 nup107-tomato::natMX4 rad11-Cerulean::hphMX leu1-32 ura4-D18*
FY9447	*h⁺ cdc21-M68-ts-dg::ura4⁺ nup107-tomato::natMX4 rad11-Cerulean::hphMX leu1-32 ura4-D18*

MATERIALS AND METHODS

Yeast strains and media. *S. pombe* strains (Table 2) were grown in supplemented Edinburgh minimal medium (EMM). Cells were incubated at 36°C for 4 h or pretreated with 12 mM hydroxyurea (HU; Sigma) for 2 h at 25°C and then incubated at 36°C for 4 h for imaging. Asynchronous cultures were placed at 36°C for 4 h, and the same number of cells were plated onto a yeast extract-sucrose (YES) plate and grown at 25°C. For calculating viability, the number of colonies grown after a 36°C pulse was normalized to the number of colonies grown from the initial culture.

Microscopy. Cells cultured in supplemented EMM were placed on 2% agarose pads sealed with VaLaP (1/1/1 [wt/wt/wt] Vaseline-lanolin-paraffin) for live-cell imaging or fixed in 70% ethanol and

incubated in 1 μg/ml DAPI (4′,6-diamidino-2-phenylindole). Images were acquired using a DeltaVision microscope (with softWoRx version 4.1; GE, Issaquah, WA) using a 60× (1.4-numerical-aperture [NA] PlanApo) lens, a solid-state illuminator, and a 12-bit charge-coupled-device (CCD) camera. Images were deconvolved, and the maximum intensities projected for fluorescence images (softWoRx) and transmitted light images were inverted and added for outlining of the cells (ImageJ) (82). Static images were projected from nine z-stacks of 0.5 μm with a 0.08- to 0.5-s exposure time. For time-lapse imaging, cells were maintained in a chamber at a constant temperature (36°C) and imaged with a shorter exposure time (0.08 s) and seven z-stacks to reduce phototoxicity.

Western blotting. Cells in supplemented EMM were collected, and the whole-cell protein extract was prepared by vortexing acid-washed glass beads in 20% trichloroacetic acid (TCA) and washing the beads with 5% TCA. Chromatin fractionation was performed after lysis with 1 mg/ml of a lysing enzyme (catalog number L1412; Sigma) and 1 mg/ml of Zymolyase 100T as described previously (83). Lysates were boiled for 5 min in Laemmli sample buffer (4% SDS, 60 mM Tris-HCl [pH 6.8], 5% glycerol, 5% 2-mercaptoethanol, 0.01% bromophenol blue) and analyzed by SDS-PAGE. Primary antibodies used were antihemagglutinin (anti-HA) (catalog number 901516; BioLegend) (1:1,000), anti-Myc (catalog number 05-419; EMD Millipore) (1:1,000), anti-phospho-H2A (catalog number 17353 [Abcam] or 05-636 [Upstate]) (1:1,000), anti-H2A (catalog number 13923; Abcam) (1:1,000), and anti-Cdc2 (gift from the Nurse laboratory) (1:4,000), as a loading control. After secondary antibody (Alexa Fluor 488 or 647) (1:4,000) incubation, blots were developed using an Amersham Typhoon biomolecular imager.

Mutation analysis. Strains with the ChL minichromosome were grown as described previously (12, 38, 84). Cultures were incubated at 36°C for 4 h and then plated and grown at 25°C. Ura-negative (Ura^-) colonies were counted, replica plated, and assessed for Leu^-, Ade^-, and hygromycin status. The minichromosome loss rate was calculated from the number of Leu^- Ura^- cells. The gross chromosomal rearrangement (GCR) rate was calculated from the numbers of Leu-positive (Leu^+) Ura^- Ade^- and Ura^- Ade^- hygromycin-resistant cells. Both mutation rates were determined by fluctuation analysis based on the Lea-Coulson method (85). A Mann-Whitney two-tailed U test was used to assess significance.

Statistical analysis. Two-tailed Student's *t* test was used to determine significance unless otherwise noted. Error bars represent standard errors (SE).

Data availability. Strains and plasmids are available upon request. We affirm that all data necessary for confirming the conclusions of the article are present within the article, figures, and tables.

SUPPLEMENTAL MATERIAL

Supplemental material is available online only.

SUPPLEMENTAL FILE 1, AVI file, 0.4 MB.

SUPPLEMENTAL FILE 2, AVI file, 0.2 MB.

ACKNOWLEDGMENTS

We thank Ji-Ping Yuan for technical support, Chance Jones for initial work on pKu70-citrine, and members of the laboratory for helpful discussions.

This work was supported by NIH grant R35-GM118109 (S.L.F.). We have no competing interests to declare.

REFERENCES

1. Neelsen KJ, Lopes M. 2015. Replication fork reversal in eukaryotes: from dead end to dynamic response. Nat Rev Mol Cell Biol 16:207–220. https://doi.org/10.1038/nrm3935.
2. Zeman MK, Cimprich KA. 2014. Causes and consequences of replication stress. Nat Cell Biol 16:2–9. https://doi.org/10.1038/ncb2897.
3. Gaillard H, García-Muse T, Aguilera A. 2015. Replication stress and cancer. Nat Rev Cancer 15:276–289. https://doi.org/10.1038/nrc3916.
4. Bell SD, Botchan MR. 2013. The minichromosome maintenance replicative helicase. Cold Spring Harb Perspect Biol 5:a012807. https://doi.org/10.1101/cshperspect.a012807.
5. Bagley BN, Keane TM, Maklakova VI, Marshall JG, Lester RA, Cancel MM, Paulsen AR, Bendzick LE, Been RA, Kogan SC, Cormier RT, Kendziorski C, Adams DJ, Collier LS. 2012. A dominantly acting murine allele of Mcm4 causes chromosomal abnormalities and promotes tumorigenesis. PLoS Genet 8:e1003034. https://doi.org/10.1371/journal.pgen.1003034.
6. Giaginis C, Vgenopoulou S, Vielh P, Theocharis S. 2010. MCM proteins as diagnostic and prognostic tumor markers in the clinical setting. Histol Histopathol 25:351–370. https://doi.org/10.14670/HH-25.351.
7. Shima N, Alcaraz A, Liachko I, Buske TR, Andrews CA, Munroe RJ, Hartford SA, Tye BK, Schimenti JC. 2007. A viable allele of Mcm4 causes chromosome instability and mammary adenocarcinomas in mice. Nat Genet 39:93–98. https://doi.org/10.1038/ng1936.
8. Casey JP, Nobbs M, McGettigan P, Lynch S, Ennis S. 2012. Recessive mutations in MCM4/PRKDC cause a novel syndrome involving a primary immunodeficiency and a disorder of DNA repair. J Med Genet 49:242–246. https://doi.org/10.1136/jmedgenet-2012-100803.
9. Hughes CR, Guasti L, Meimaridou E, Chuang C, Schimenti JC, King PJ, Costigan C, Clark AJL, Metherell LA. 2012. MCM4 mutation causes adrenal failure, short stature, and natural killer cell deficiency in humans. J Clin Invest 122:814–820. https://doi.org/10.1172/JCI60224.
10. Gineau L, Cognet C, Kara N, Lach FP, Dunne J, Veturi U, Picard C, Trouillet C, Eidenschenk C, Aoufouchi S, Alcaïs A, Smith O, Geissmann F, Feighery C, Abel L, Smogorzewska A, Stillman B, Vivier E, Casanova J-L, Jouanguy E. 2012. Partial MCM4 deficiency in patients with growth retardation, adrenal insufficiency, and natural killer cell deficiency. J Clin Invest 122:821–832. https://doi.org/10.1172/JCI61014.
11. Ranatunga NS, Forsburg SL. 2016. Characterization of a novel MMS-sensitive allele of Schizosaccharomyces pombe mcm4. G3 (Bethesda) 6:3049–3063. https://doi.org/10.1534/g3.116.033571.
12. Sabatinos SA, Ranatunga NS, Yuan J, Green MD, Forsburg SL, Solomon MJ. 2015. Replication stress in early S phase generates apparent micronuclei and chromosome rearrangement in fission yeast. Mol Biol Cell 26:3439–3450. https://doi.org/10.1091/mbc.E15-05-0318.
13. Coxon A, Maundrell K, Kearsey SE. 1992. Fission yeast cdc21+ belongs to a family of proteins involved in an early step of chromosome replication. Nucleic Acids Res 20:5571–5577. https://doi.org/10.1093/nar/20.21.5571.
14. Nitani N, Yadani C, Yabuuchi H, Masukata H, Nakagawa T. 2008. Mcm4 C-terminal domain of MCM helicase prevents excessive formation of

single-stranded DNA at stalled replication forks. Proc Natl Acad Sci U S A 105:12973–12978. https://doi.org/10.1073/pnas.0805307105.
15. Nasmyth K, Nurse P. 1981. Cell division cycle mutants altered in DNA replication and mitosis in the fission yeast Schizosaccharomyces pombe. Mol Gen Genet 182:119–124. https://doi.org/10.1007/bf00422777.
16. Maiorano D, Van Assendelft GB, Kearsey SE. 1996. Fission yeast cdc21, a member of the MCM protein family, is required for onset of S phase and is located in the nucleus throughout the cell cycle. EMBO J 15:861–872. https://doi.org/10.1002/j.1460-2075.1996.tb00421.x.
17. Bailis JM, Luche DD, Hunter T, Forsburg SL. 2008. Minichromosome maintenance proteins interact with checkpoint and recombination proteins to promote S-phase genome stability. Mol Cell Biol 28:1724–1738. https://doi.org/10.1128/MCB.01717-07.
18. Lindner K, Grega J, Montgomery S, Kearsey SE. 2002. Essential role of MCM proteins in premeiotic DNA replication. Mol Biol Cell 13:435–444. https://doi.org/10.1091/mbc.01-11-0537.
19. Ira G, Pellicioli A, Balijja A, Wang X, Fiorani S, Carotenuto W, Liberi G, Bressan D, Wan L, Hollingsworth NM, Haber JE, Foiani M. 2004. DNA end resection, homologous recombination and DNA damage checkpoint activation require CDK1. Nature 431:1011–1017. https://doi.org/10.1038/nature02964.
20. Hu J, Sun L, Shen F, Chen Y, Hua Y, Liu Y, Zhang M, Hu Y, Wang Q, Xu W, Sun F, Ji J, Murray JM, Carr AM, Kong D. 2012. The intra-S phase checkpoint targets Dna2 to prevent stalled replication forks from reversing. Cell 149:1221–1232. https://doi.org/10.1016/j.cell.2012.04.030.
21. Lopes M, Foiani M, Sogo JM. 2006. Multiple mechanisms control chromosome integrity after replication fork uncoupling and restart at irreparable UV lesions. Mol Cell 21:15–27. https://doi.org/10.1016/j.molcel.2005.11.015.
22. Byun TS, Pacek M, Yee M, Walter JC, Cimprich KA. 2005. Functional uncoupling of MCM helicase and DNA polymerase activities activates the ATR-dependent checkpoint. Genes Dev 19:1040–1052. https://doi.org/10.1101/gad.1301205.
23. Branzei D, Foiani M. 2010. Maintaining genome stability at the replication fork. Nat Rev Mol Cell Biol 11:208–219. https://doi.org/10.1038/nrm2852.
24. Lindsay HD, Griffiths DJF, Edwards RJ, Christensen PU, Murray JM, Osman F, Walworth N, Carr AM. 1998. S-phase-specific activation of Cds1 kinase defines a subpathway of the checkpoint response in Schizosaccharomyces pombe. Genes Dev 12:382–395. https://doi.org/10.1101/gad.12.3.382.
25. Boddy MN, Furnari B, Mondesert O, Russell P. 1998. Replication checkpoint enforced by kinases Cds1 and Chk1. Science 280:909–912. https://doi.org/10.1126/science.280.5365.909.
26. Rhind N, Russell P. 1998. The Schizosaccharomyces pombe S-phase checkpoint differentiates between different types of DNA damage. Genetics 149:1729–1737.
27. Giannattasio M, Branzei D. 2017. S-phase checkpoint regulations that preserve replication and chromosome integrity upon dNTP depletion. Cell Mol Life Sci 74:2361–2380. https://doi.org/10.1007/s00018-017-2474-4.
28. Rhind N, Russell P. 2000. Chk1 and Cds1: linchpins of the DNA damage and replication checkpoint pathways. J Cell Sci 113:3889–3896.
29. Xu Y, Davenport M, Kelly TJ. 2006. Two-stage mechanism for activation of the DNA replication checkpoint kinase Cds1 in fission yeast. Genes Dev 20:990–1003. https://doi.org/10.1101/gad.1406706.
30. Barnum KJ, O'Connell MJ. 2014. Cell cycle regulation by checkpoints. Methods Mol Biol 1170:29–40. https://doi.org/10.1007/978-1-4939-0888-2_2.
31. Boddy MN, Gaillard PL, McDonald WH, Shanahan P, Yates JR, III, Russell P. 2001. Mus81-Eme1 are essential components of a Holliday junction resolvase. Cell 107:537–548. https://doi.org/10.1016/S0092-8674(01)00536-0.
32. Hanada K, Budzowska M, Modesti M, Maas A, Wyman C, Essers J, Kanaar R. 2006. The structure-specific endonuclease Mus81-Eme1 promotes conversion of interstrand DNA crosslinks into double-strands breaks. EMBO J 25:4921–4932. https://doi.org/10.1038/sj.emboj.7601344.
33. Kai M, Boddy MN, Russell P, Wang TS. 2005. Replication checkpoint kinase Cds1 regulates Mus81 to preserve genome integrity during replication stress. Genes Dev 19:919–932. https://doi.org/10.1101/gad.1304305.
34. Kim SM, Forsburg SL. 2018. Regulation of structure-specific endonucleases in replication stress. Genes (Basel) 9:634. https://doi.org/10.3390/genes9120634.
35. Pfander B, Matos J. 2017. Control of Mus81 nuclease during the cell cycle. FEBS Lett 591:2048–2056. https://doi.org/10.1002/1873-3468.12727.
36. Carr AM, Moudjou M, Bentley NJ, Hagan IM. 1995. The chk1 pathway is required to prevent mitosis following cell-cycle arrest at 'start'. Curr Biol 5:1179–1190. https://doi.org/10.1016/s0960-9822(95)00234-x.
37. Boddy MN, Lopez-Girona A, Shanahan P, Interthal H, Heyer W-D, Russell P. 2000. Damage tolerance protein Mus81 associates with the FHA1 domain of checkpoint kinase Cds1. Mol Cell Biol 20:8758–8766. https://doi.org/10.1128/mcb.20.23.8758-8766.2000.
38. Nakamura K, Okamoto A, Katou Y, Yadani C, Shitanda T, Kaweeteerawat C, Takahashi TS, Itoh T, Shirahige K, Masukata H, Nakagawa T. 2008. Rad51 suppresses gross chromosomal Schizosaccharomyces pombe. EMBO J 27:3036–3046. https://doi.org/10.1038/emboj.2008.215.
39. Nakamura TM, Du L-L, Redon C, Russell P. 2004. Histone H2A phosphorylation controls Crb2 recruitment at DNA breaks, maintains checkpoint arrest, and influences DNA repair in fission yeast. Mol Cell Biol 24:6215–6230. https://doi.org/10.1128/MCB.24.14.6215-6230.2004.
40. Lai X, Broderick R, Bergoglio V, Zimmer J, Badie S, Niedzwiedz W, Hoffmann J-S, Tarsounas M. 2017. Mus81 nuclease activity is essential for replication stress tolerance and chromosome segregation in BRCA2-deficient cells. Nat Commun 8:15983. https://doi.org/10.1038/ncomms15983.
41. Hanada K, Budzowska M, Davies SL, van Drunen E, Onizawa H, Beverloo HB, Maas A, Essers J, Hickson ID, Kanaar R. 2007. The structure-specific endonuclease Mus81 contributes to replication restart by generating double-strand DNA breaks. Nat Struct Mol Biol 14:1096–1104. https://doi.org/10.1038/nsmb1313.
42. Regairaz M, Zhang Y, Fu H, Agama KK, Tata N, Agrawal S, Aladjem MI, Pommier Y. 2011. Mus81-mediated DNA cleavage resolves replication forks stalled by topoisomerase I-DNA complexes. J Cell Biol 195:739–749. https://doi.org/10.1083/jcb.201104003.
43. Ciccia A, Constantinou A, West SC. 2003. Identification and characterization of the human Mus81-Eme1 endonuclease. J Biol Chem 278:25172–25178. https://doi.org/10.1074/jbc.M302882200.
44. Shibata A, Jeggo P, Löbrich M. 2018. The pendulum of the Ku-Ku clock. DNA Repair (Amst) 71:164–171. https://doi.org/10.1016/j.dnarep.2018.08.020.
45. Fell VL, Schild-Poulter C. 2015. The Ku heterodimer: function in DNA repair and beyond. Mutat Res Rev Mutat Res 763:15–29. https://doi.org/10.1016/j.mrrev.2014.06.002.
46. Mahaney BL, Meek K, Lees-Miller SP. 2009. Repair of ionizing radiation-induced DNA double-strand breaks by non-homologous end-joining. Biochem J 417:639–650. https://doi.org/10.1042/BJ20080413.
47. Foster SS, Balestrini A, Petrini JHJ. 2011. Functional interplay of the Mre11 nuclease and Ku in the response to replication-associated DNA damage. Mol Cell Biol 31:4379–4389. https://doi.org/10.1128/MCB.05854-11.
48. Langerak P, Mejia-Ramirez E, Limbo O, Russell P. 2011. Release of Ku and MRN from DNA ends by Mre11 nuclease activity and Ctp1 is required for homologous recombination repair of double-strand breaks. PLoS Genet 7:e1002271. https://doi.org/10.1371/journal.pgen.1002271.
49. Teixeira-Silva A, Saada AA, Hardy J, Iraqui I, Nocente MC, Fréon K, Lambert SAE. 2017. The end-joining factor Ku acts in the end-resection of double strand break-free arrested replication forks. Nat Commun 8:1982. https://doi.org/10.1038/s41467-017-02144-5.
50. Gould KL, Simanis V. 1997. The control of septum formation in fission yeast. Genes Dev 11:2939–2951. https://doi.org/10.1101/gad.11.22.2939.
51. Oza P, Jaspersen SL, Miele A, Dekker J, Peterson CL. 2009. Mechanisms that regulate localization of a DNA double-strand break to the nuclear periphery. Genes Dev 23:912–927. https://doi.org/10.1101/gad.1782209.
52. Freudenreich CH, Su XA. 2016. Relocalization of DNA lesions to the nuclear pore complex. FEMS Yeast Res 16:fow095. https://doi.org/10.1093/femsyr/fow095.
53. Chu Z, Eshaghi M, Poon SY, Liu J. 2009. A Cds1-mediated checkpoint protects the MBF activator Rep2 from ubiquitination by anaphase-promoting complex/cyclosome–Ste9 at S-phase arrest in fission yeast. Mol Cell Biol 29:4959–4970. https://doi.org/10.1128/MCB.00562-09.
54. Bastos de Oliveira FM, Harris MR, Brazauskas P, de Bruin RAM, Smolka MB. 2012. Linking DNA replication checkpoint to MBF cell-cycle transcription reveals a distinct class of G1/S genes. EMBO J 31:1798–1810. https://doi.org/10.1038/emboj.2012.27.
55. Dutta C, Patel PK, Rosebrock A, Oliva A, Leatherwood J, Rhind N. 2008. The DNA replication checkpoint directly regulates MBF-dependent G_1/S

transcription. Mol Cell Biol 28:5977–5985. https://doi.org/10.1128/MCB.00596-08.
56. de Bruin RAM, Kalashnikova TI, Aslanian A, Wohlschlegel J, Chahwan C, Yates JR, III, Russell P, Wittenberg C. 2008. DNA replication checkpoint promotes G1-S transcription by inactivating the MBF repressor Nrm1. Proc Natl Acad Sci U S A 105:11230–11235. https://doi.org/10.1073/pnas.0801106105.
57. Kiang L, Heichinger C, Watt S, Bähler J, Nurse P. 2009. Cyclin-dependent kinase inhibits reinitiation of a normal S-phase program during G_2 in fission yeast. Mol Cell Biol 29:4025–4032. https://doi.org/10.1128/MCB.00185-09.
58. Kim SM, Tripathi VP, Shen K-F, Forsburg SL. 2020. Checkpoint regulation of nuclear Tos4 defines S phase arrest in fission yeast. G3 (Bethesda) 10:255–266. https://doi.org/10.1534/g3.119.400726.
59. Froget B, Blaisonneau J, Lambert S, Baldacci G. 2008. Cleavage of stalled forks by fission yeast Mus81/Eme1 in absence of DNA replication checkpoint. Mol Biol Cell 19:445–456. https://doi.org/10.1091/mbc.e07-07-0728.
60. Reichard P. 1988. Interactions between deoxyribonucleotide and DNA synthesis. Annu Rev Biochem 57:349–374. https://doi.org/10.1146/annurev.bi.57.070188.002025.
61. Kai M, Wang TS. 2003. Checkpoint activation regulates mutagenic translesion synthesis. Genes Dev 17:64–76. https://doi.org/10.1101/gad.1043203.
62. Sabatinos SA, Green MD, Forsburg SL. 2012. Continued DNA synthesis in replication checkpoint mutants leads to fork collapse. Mol Cell Biol 32:4986–4997. https://doi.org/10.1128/MCB.01060-12.
63. Meister P, Taddei A, Ponti A, Baldacci G, Gasser SM. 2007. Replication foci dynamics: replication patterns are modulated by S-phase checkpoint kinases in fission yeast. EMBO J 26:1315–1326. https://doi.org/10.1038/sj.emboj.7601538.
64. Falquet B, Rass U. 2019. Structure-specific endonucleases and the resolution of chromosome underreplication. Genes (Basel) 10:232. https://doi.org/10.3390/genes10030232.
65. Zou L, Elledge SJ. 2003. Sensing DNA damage through ATRIP recognition of RPA-ssDNA complexes. Science 300:1542–1548. https://doi.org/10.1126/science.1083430.
66. Shechter D, Costanzo V, Gautier J. 2004. ATR and ATM regulate the timing of DNA replication origin firing. Nat Cell Biol 6:648–655. https://doi.org/10.1038/ncb1145.
67. Gonzalez Besteiro MA, Gottifredi V. 2015. The fork and the kinase: a DNA replication tale from a CHK1 perspective. Mutat Res Rev Mutat Res 763:168–180. https://doi.org/10.1016/j.mrrev.2014.10.003.
68. MacDougall CA, Byun TS, Van C, Yee M, Cimprich KA. 2007. The structural determinants of checkpoint activation. Genes Dev 21:898–903. https://doi.org/10.1101/gad.1522607.
69. Van C, Yan S, Michael WM, Waga S, Cimprich KA. 2010. Continued primer synthesis at stalled replication forks contributes to checkpoint activation. J Cell Biol 189:233–246. https://doi.org/10.1083/jcb.200909105.
70. Chan YW, Fugger K, West SC. 2018. Unresolved recombination intermediates lead to ultra-fine anaphase bridges, chromosome breaks and aberrations. Nat Cell Biol 20:92–103. https://doi.org/10.1038/s41556-017-0011-1.
71. Ait Saada A, Lambert SAE, Carr AM. 2018. Preserving replication fork integrity and competence via the homologous recombination pathway. DNA Repair (Amst) 71:135–147. https://doi.org/10.1016/j.dnarep.2018.08.017.
72. Ryu T, Spatola B, Delabaere L, Bowlin K, Hopp H, Kunitake R, Karpen GH, Chiolo I. 2015. Heterochromatic breaks move to the nuclear periphery to continue recombinational repair. Nat Cell Biol 17:1401–1411. https://doi.org/10.1038/ncb3258.
73. Caridi CP, Agostino CD, Ryu T, Zapotoczny G, Delabaere L, Li X, Khodaverdian VY, Amaral N, Lin E, Rau AR, Chiolo I. 2018. Nuclear F-actin and myosins drive relocalization of heterochromatic breaks. Nature 559:54–60. https://doi.org/10.1038/s41586-018-0242-8.
74. Lisby M, Barlow JH, Burgess RC, Rothstein R. 2004. Choreography of the DNA damage response: spatiotemporal relationships among checkpoint and repair proteins. Cell 118:699–713. https://doi.org/10.1016/j.cell.2004.08.015.
75. Oshidari R, Huang R, Medghalchi M, Tse EYW, Ashgriz N, Lee HO, Wyatt H, Mekhail K. 2020. DNA repair by Rad52 liquid droplets. Nat Commun 11:695. https://doi.org/10.1038/s41467-020-14546-z.
76. Ferreira MG, Cooper JP. 2004. Two modes of DNA double-strand break repair are reciprocally regulated through the fission yeast cell cycle. Genes Dev 18:2249–2254. https://doi.org/10.1101/gad.315804.
77. Caspari T, Murray JM, Carr AM. 2002. Cdc2-cyclin B kinase activity links Crb2 and Rqh1-topoisomerase III. Genes Dev 16:1195–1208. https://doi.org/10.1101/gad.221402.
78. Shao Z, Davis AJ, Fattah KR, So S, Sun J, Lee K-J, Harrison L, Yang J, Chen DJ. 2012. Persistently bound Ku at DNA ends attenuates DNA end resection and homologous recombination. DNA Repair (Amst) 11:310–316. https://doi.org/10.1016/j.dnarep.2011.12.007.
79. Myler LR, Gallardo IF, Soniat MM, Deshpande RA, Gonzalez XB, Kim Y, Paull TT, Finkelstein IJ. 2017. Single-molecule imaging reveals how Mre11-Rad50-Nbs1 initiates DNA break repair. Mol Cell 67:891–898.e4. https://doi.org/10.1016/j.molcel.2017.08.002.
80. Chanut P, Britton S, Coates J, Jackson SP, Calsou P. 2016. Coordinated nuclease activities counteract Ku at single-ended DNA double-strand breaks. Nat Commun 7:12889. https://doi.org/10.1038/ncomms12889.
81. Wang W, Daley JM, Kwon Y, Xue X, Krasner DS, Miller AS, Nguyen KA, Williamson EA, Shim EY, Lee SE, Hromas R, Sung P. 2018. A DNA nick at Ku-blocked double-strand break ends serves as an entry site for exonuclease 1 (Exo1) or Sgs1-Dna2 in long-range DNA end resection. J Biol Chem 293:17061–17069. https://doi.org/10.1074/jbc.RA118.004769.
82. Schindelin J, Arganda-Carreras I, Frise E, Kaynig V, Longair M, Pietzsch T, Preibisch S, Rueden C, Saalfeld S, Schmid B, Tinevez J, White DJ, Hartenstein V, Eliceiri K, Tomancak P, Cardona A. 2012. Fiji: an open-source platform for biological-image analysis. Nat Methods 9:676–682. https://doi.org/10.1038/nmeth.2019.
83. Kunoh T, Habu T. 2014. Chromatin fractionation assay in fission yeast. Bio Protoc 4:e1185. https://doi.org/10.21769/BioProtoc.1185.
84. Li P, Petreaca RC, Jensen A, Yuan J, Green MD, Forsburg SL. 2013. Replication fork stability is essential for the maintenance of centromere integrity in the absence of heterochromatin. Cell Rep 3:638–645. https://doi.org/10.1016/j.celrep.2013.02.007.
85. Foster P. 2006. Methods for determining spontaneous mutation rates. Methods Enzymol 409:195–213. https://doi.org/10.1016/S0076-6879(05)09012-9.
86. Lock A, Rutherford K, Harris MA, Hayles J, Oliver SG, Bähler J, Wood V. 2019. PomBase 2018: user-driven reimplementation of the fission yeast database provides rapid and intuitive access to diverse, interconnected information. Nucleic Acids Res 47:D821–D827. https://doi.org/10.1093/nar/gky961.